# Endothelial Progenitor Cells Control the Angiogenic Switch in Mouse Lung Metastasis

Dingcheng Gao, *et al.*

*Science* **319**, 195 (2008);
DOI: 10.1126/science.1150224

18. Materials and methods are available as supporting material on *Science* Online.
19. T. P. Young, B. D. Okello, D. Kinyua, T. M. Palmer, *Afr. J. Range Forage Sci.* **14**, 94 (1998).
20. M. Huntzinger, R. Karban, T. P. Young, T. M. Palmer, *Ecology* **85**, 609 (2004).
21. T. P. Young, M. L. Stanton, C. E. Christian, *Oikos* **101**, 171 (2003).
22. T. M. Palmer, *Ecology* **84**, 2843 (2003).
23. B. J. Peterson, B. Fry, *Annu. Rev. Ecol. Syst.* **18**, 293 (1987).
24. D. M. Post, *Ecology* **83**, 703 (2002).
25. M. L. Stanton, T. M. Palmer, T. P. Young, *Ecol. Monogr.* **72**, 347 (2002).
26. R. M. Pringle, T. P. Young, D. I. Rubenstein, D. J. McCauley, *Proc. Natl. Acad. Sci. U.S.A.* **104**, 193 (2007).
27. E. G. Brockerhoff, A. M. Liebhold, H. Jactel, *Can. J. For. Res.* **36**, 263 (2006).
28. D. W. Davidson, *Biol. J. Linn. Soc.* **61**, 153 (1997).
29. J. T. Du Toit, D. H. M. Cumming, *Biodiversity Conserv.* **8**, 1643 (1999).
30. W. K. Ottichilo, J. De Leeuw, A. K. Skidmore, H. H. T. Prins, M. Y. Said, *Afr. J. Ecol.* **38**, 202 (2000).
31. We thank J. Lemboi and the excellent staff at Mpala Research Centre and Mpala Ranch for logistical support, students from The Kenya Wildlands Program for field assistance, and the Gordon Lab (Stanford University), Koch Lab (University of California), Silliman Lab (University of Florida), K. Rudolph, and four anonymous reviewers for helpful comments on the manuscript. This work was funded by NSF grants DEB-0089706 and DEB-0444741 to T.M.P., M.L.S., and T.P.Y. The KLEE plots were built and maintained with grants from the James Smithson Fund of the Smithsonian Institution (to A. Smith), the National Geographic Society (4691-91), NSF (BSR-97-07477 and BSR-03-16402), and the African Elephant Program of the U.S. Fish and Wildlife Service (98210-0G563) (to T.P.Y.). This research was carried out under the auspices of the Ministry of Education, Science, and Technology of the Republic of Kenya (Permit number MOEST 13/001/34 17). This paper is dedicated to the memory of Otis Trout Palmer, a true mutualist.

**Supporting Online Material**
www.sciencemag.org/cgi/content/full/319/5860/192/DC1
Materials and Methods
Fig. S1
References

10 October 2007; accepted 28 November 2007
10.1126/science.1151579

# Endothelial Progenitor Cells Control the Angiogenic Switch in Mouse Lung Metastasis

**Dingcheng Gao, Daniel J. Nolan, Albert S. Mellick, Kathryn Bambino, Kevin McDonnell, Vivek Mittal***

**Angiogenesis-mediated progression of micrometastasis to lethal macrometastasis is the major cause of death in cancer patients. Here, using mouse models of pulmonary metastasis, we identify bone marrow (BM)–derived endothelial progenitor cells (EPCs) as critical regulators of this angiogenic switch. We show that tumors induce expression of the transcription factor Id1 in the EPCs and that suppression of Id1 after metastatic colonization blocked EPC mobilization, caused angiogenesis inhibition, impaired pulmonary macrometastases, and increased survival of tumor-bearing animals. These findings establish the role of EPCs in metastatic progression in preclinical models and suggest that selective targeting of EPCs may merit investigation as a therapy for cancer patients with lung metastases.**

Disseminated malignant primary tumor cells colonize target secondary organs, through bone marrow (BM)–derived premetastatic niches (*1*, *2*), to form dormant micrometastases (*3*). In some cases, these micrometastases activate the angiogenic switch and progress to macrometastases (*4*, *5*). The cellular and molecular mechanisms regulating the angiogenic switch and the dynamics of vessel assembly during the progression of micrometastases to macrometastases remain poorly understood, which limits the utility of antiangiogenic approaches to controlling metastasis. In this study, we have investigated whether BM-derived endothelial progenitor cells (EPCs) contribute to angiogenesis-mediated progression of micrometastases into deadly macrometastases.

To facilitate tracking of both metastatic tumor cells and BM-derived cells in vivo, we implanted Lewis lung carcinoma cells stably expressing red fluorescent protein (LLC-RFP) into syngeneic mice reconstituted with BM cells expressing green fluorescent protein ($GFP^+$ BM) (fig. S1A) (*6*). After primary tumor resection (fig. S1B), numerous $RFP^+$ pulmonary micrometastases (<1 mm in diameter) were detected by stereomicroscopic imaging at day 14 after tumor inoculation (12 on average per animal) (fig. S1C). The total number of metastases increased with time (average 22 and 35 per animal at day 21 and day 28, respectively) (Fig. 1A), with a concomitant increase in macrometastases (≥1 mm in diameter, 47% at day 28) (Fig. 1A), which indicated a time window of micrometastasis to macrometastasis progression. We next determined whether this window of metastasis progression was associated with the angiogenic switch. Immunohistochemical staining showed that the micrometastatic foci (day 14) were largely avascular, as determined by a lack of $CD31^+$ vessels (Fig. 1B, top). In contrast, macrometastatic foci (days 21 to 28) were infiltrated with many $CD31^+$ neovessels of various sizes (Fig. 1B, bottom), which suggested that these lesions had undergone an angiogenic switch during their expansion in size. As expected, many BM-derived $GFP^+$ cells were recruited to both micro- and macrometastases (fig. S1C and Fig. 1B). Although a majority of these cells represented hematopoietic lineages, as previously described in primary tumors (*7*) (fig. S2A), we focused on BM-derived endothelial cells that directly contribute to neovascularization (*8*). Microscopic analysis of macrometastases showed that a subset of neovessels had incorporated BM-derived endothelial cells [$GFP^+CD31^+$ (Fig. 1C)]. Luminal incorporation was confirmed by optical sectioning microscopy, which showed that the GFP and CD31 signals were localized to the same individual cell in all three dimensions [supporting online material (SOM) text, Note 1, and (fig. S2B)]. Functional incorporation of BM-derived endothelial cells was quantified by systemic perfusion of fluorescently labeled isolectin GS-IB4, which specifically binds to the luminal surface of endothelial cells in vessels with active blood circulation (*8*, *9*). Macrometastases were dissected from the lungs, and fluorescence activated cell sorting (FACS) analysis showed that the luminally incorporated BM-derived endothelial cells ($GFP^+Lectin^+CD31^+CD11b^-$) represent on average 12.7 ± 2.9% of total endothelial cells ($Lectin^+CD31^+CD11b^-$) (Fig. 1, D and E).

To confirm that these events also occur in a model of spontaneous metastasis, we transplanted syngeneic $GFP^+$ BM into MMTV-PyMT transgenic mice, a model of breast cancer. Pulmonary micrometastases were detected in the mice at 12 weeks of age, and these lesions progressed into numerous macrometastases by week 16 (Fig. 2A). Notably, $GFP^+$ BM-derived cells colocalized with the metastatic lesions (Fig. 2B). As observed in the LLC model, the micrometastases were avascular and lacked $CD31^+$ vessels (Fig. 2C), whereas macrometastases were infiltrated by $CD31^+$ neovessels (Fig. 2D), which indicated that these lesions had undergone an angiogenic switch at this defined window. Histology revealed vessel-incorporated $GFP^+$ $CD31^+$ BM-derived endothelial cells (Fig. 2E). Further quantification showed that 11.7 ± 3.7% of vessels in the metastases contained incorporated $GFP^+$ BM-derived endothelial cells (Fig. 2F).

We have previously shown that the BM-derived endothelial cells are derived from progenitor cells defined by cell surface expression of vascular endothelial (VE)–cadherin, vascular endothelial growth factor receptor 2 (VEGFR2), dim CD31, and Prominin I and lack various hematopoietic markers (*8*). Analysis of micrometastases showed infiltration of BM-derived $GFP^+$ VE-$cadherin^+$ EPCs in the peripheral region of the lesions (Fig. 3A). FACS analysis of the lungs bearing micro-

Cancer Genome Research Center, Cold Spring Harbor Laboratory, Cold Spring Harbor, NY 11724, USA.

*To whom correspondence should be addressed. E-mail: mittal@cshl.edu

metastases showed a fivefold increase in BM-derived EPCs ($GFP^+$ VE-cadherin$^+$ $CD31^{dim}$ $CD11b^-$), as compared with that of control normal lungs (198.5 ± 29.9 versus 37.3 ± 6.1, $P < 0.0001$) (Fig. 3, B and C). To determine the mechanism underlying EPC recruitment to the sites of neovascularization, we examined metastatic lesions for the expression of adhesion molecules. Nascent vessels confined to the metastatic lesions expressed higher levels of vascular cell adhesion molecule–1 (VCAM-1), and notably, EPCs expressed cognate receptors integrin $\alpha_4\beta_1$ (fig. S3, A, C, and D). Indeed, the presence of EPCs in the proximity of VCAM-1$^+$ vessels (fig. S3B) suggests that interactions between VCAM-1 and integrin $\alpha_4\beta_1$ mediate EPC recruitment, as observed previously for hematopoietic progenitors (*10*–*12*). Taken together, these results demonstrate that an angiogenic switch is associated with the progression of micrometastases to macrometastases, during which BM-derived EPCs are recruited to the metastatic foci and contribute luminally to the neovasculature in metastatic lesions.

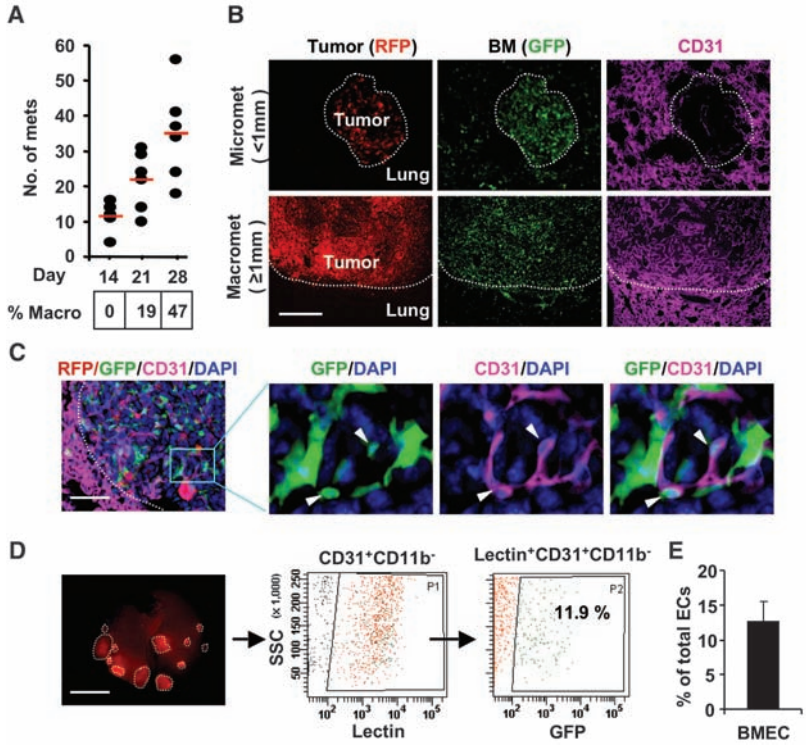


**Fig. 1.** BM-derived endothelial cells contribute to the angiogenic switch in mice transplanted with LLC cells. (**A**) Quantification of total metastatic colonies in the lung after tumor inoculation. The percentage of macrometastases (≥1 mm in diameter) is indicated; $n$ = 6 per time point. (**B**) Microscopy showing avascular micrometastases (top, day 14) and a vascularized macrometastasis (bottom, day 21). Blood vessels were detected by CD31-specific antibody. Dotted line separates the host tissue from the tumor in this and subsequent figures. Scale bar, 200 μm. (**C**) Vessel incorporated BM-derived endothelial cells ($GFP^+$ $CD31^+$, arrows) in $RFP^+$ macrometastasis stained with DAPI (4′,6′-diamidino-2-phenylindole). Scale bar, 100 μm. (**D**) Scatter plot depicting contribution of BM-derived endothelial cells in functional vessels of microdissected macrometastasis. P1 gate, total functional endothelial cells ($CD31^+$ Isolectin$^+$ $CD11b^-$); P2 gate, BM-derived endothelial cells ($GFP^+$ $CD31^+$ Isolectin$^+$ $CD11b^-$). Results obtained by analyzing $1 \times 10^6$ cells. SSC, side-scatter values. (**E**) Quantification of FACS analysis showing percentage of BM-derived endothelial cells (BMEC) in vessels of macrometastases. Data are means ± SD; $n$ = 5 per group.

To explore whether BM-derived EPCs are required for the progression of micrometastasis to macrometastasis, we studied the effects of loss of EPC function in vivo. We focused on the Id1 transcription factor because Id1 knockout mice ($Id1^{+/-}$ $Id3^{-/-}$) exhibit impaired tumor growth, because of BM-associated angiogenic defects (*13*, *14*). Notably, in response to a tumor challenge, we detected a ~2.5-fold up-regulation in Id1 mRNA expression in the BM cells (Fig. 3D). More important, Id1 expression was confined to EPCs and was not seen in other BM cells upon tumor challenge (Fig. 3E and fig. S4A), which suggests that Id1 may be critical for EPC function in the context of metastasis. To dissect the role of Id1 in EPC-mediated progression of metastatic lesions, we used a lentiviral-based synthetic microRNA (miR-30)–based short hairpin RNA (shRNA) expression system whose activity could be induced by doxycycline (Dox) to target Id1 expression in vivo (fig. S5). This approach allowed us to generate acute Id1 suppression in the BM selectively during metastasis progression without compromising the contribution of BM-derived endothelial cells to the growth of primary tumor, which cannot be achieved in the Id1 knockout

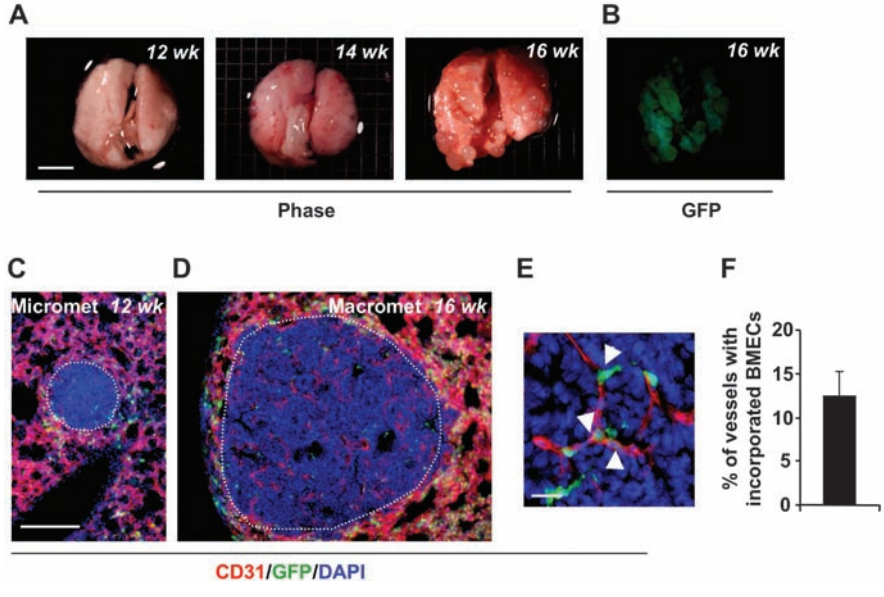


**Fig. 2.** BM-derived endothelial cells contribute to the angiogenic switch in MMTV-PyMT mice, a model of spontaneous metastasis. (**A** and **B**) Representative lung images showing metastasis progression (weeks 12 to 16) in MMTV-PyMT mice reconstituted with $GFP^+$ BM; $n$ = 20 mice. Scale bar, 5 mm. CD31 staining of pulmonary micrometastases (**C**) and macrometastases (**D**) in MMTV-PyMT mice. Dotted line, as in Fig. 1. Scale bar, 200 μm. (**E**) Incorporated BM-derived endothelial cells ($GFP^+$ $CD31^+$, arrows) in the vessels in macrometastases in MMTV-PyMT mice. Scale bar, 20 μm. (**F**) Quantification of vessels containing $GFP^+$ BM-derived endothelial cells. Data are means ± SD. (A total of 2418 vessels were counted; $n$ = 38 metastases derived from six animals).

mice. An effective shRNA that reduced endogenous Id1 mRNA and protein levels (>95% reduction) (fig. S4, B and C) was cloned into a Dox–inducible expression vector (fig. S4D). The specific and tight regulation of Id1 shRNA expression by the inducible system was established in the context of genomic integration in vitro (fig. S4, E and F).

To determine the impact of Id1 gene suppression on metastasis progression, lineage negative ($Lin^-$) cells derived from ROSA26 reverse tetracycline transactivator (rtTA) transgenic mice (*15*) were transduced ex vivo with lentivirus expressing either the Id1 shRNA or the nonspecific shRNA and transplanted into lethally irradiated recipient mice according to the scheme in fig. S5A. No significant change in primary tumor growth was observed in these animals (fig. S5B) before Dox administration. However, Dox-mediated induction of Id1 shRNA expression substantially reduced the total number of metastases in animals having an Id1 shRNA bone marrow transplant (BMT) (28 ± 6 in –Dox versus 8 ± 5 in +Dox) as compared with nonspecific shRNA-

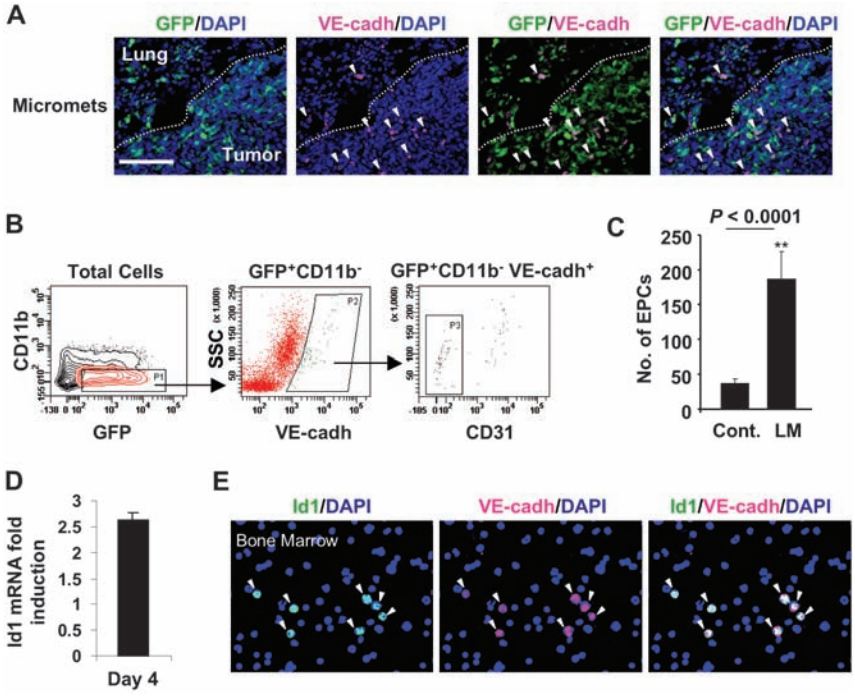


**Fig. 3.** $Id1^+$ EPCs contribute to early metastatic lesions in mice. (**A**) Microscopy showing recruitment of BM-derived EPCs ($GFP^+$ VE-$cadherin^+$) at the periphery of LLC micrometastases in the lung (day 14). Dotted line is as in Fig. 1. Scale bar, 100 μm. (**B**) FACS analysis of EPC recruitment from lungs bearing micrometastases (day 14). Of the total lung cells, BM-derived non-hematopoietic cells ($GFP^+$ $CD11b^-$) were gated (P1), from which BM-derived total endothelial cells ($GFP^+$ VE-$cadherin^+$ $CD11b^-$) were determined (P2). A subset of these cells are EPCs ($GFP^+$ VE-$cadherin^+$ $CD31^{dim}$ $CD11b^-$) represented by (P3). (**C**) Quantification of FACS analysis showing EPC recruitment to metastatic lungs (LM) (day 14) versus control lungs (Cont.). Results are from analysis of $1 \times 10^6$ cells per animal. Means ± SD; $n = 5$ per group. (**D**) Quantitative RT-PCR analysis showing Id1 mRNA levels in $Lin^-$ BM cells harvested from tumor challenged versus unchallenged mice. (**E**) Microscopy showing that Id1 expression is confined to VE-$cadherin^+$ EPCs in tumor-challenged BM (arrows).

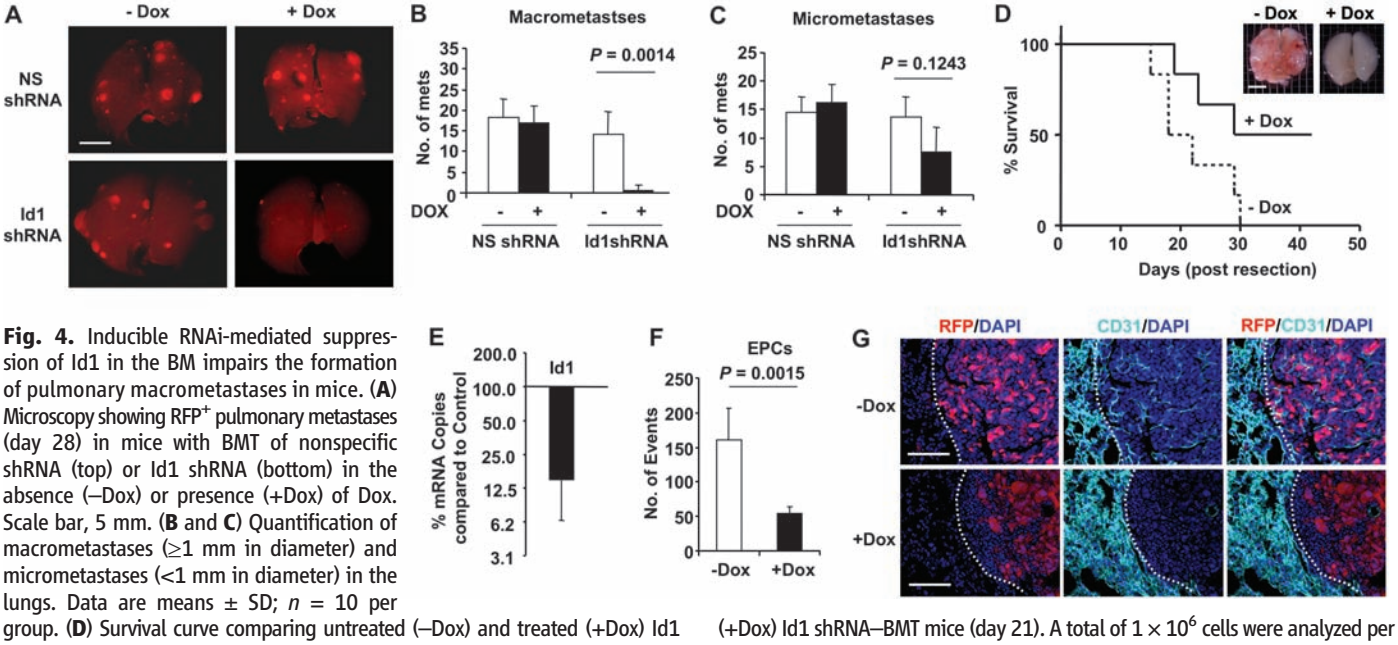


**Fig. 4.** Inducible RNAi-mediated suppression of Id1 in the BM impairs the formation of pulmonary macrometastases in mice. (**A**) Microscopy showing $RFP^+$ pulmonary metastases (day 28) in mice with BMT of nonspecific shRNA (top) or Id1 shRNA (bottom) in the absence (–Dox) or presence (+Dox) of Dox. Scale bar, 5 mm. (**B** and **C**) Quantification of macrometastases (≥1 mm in diameter) and micrometastases (<1 mm in diameter) in the lungs. Data are means ± SD; $n = 10$ per group. (**D**) Survival curve comparing untreated (–Dox) and treated (+Dox) Id1 shRNA–BMT mice. (Insets) Representative lungs isolated from –Dox (day 30 post resection) and +Dox (day 42 post resection) mice. Scale bar, 5 mm. (**E**) Quantitative RT-PCR analysis showing Id1 mRNA levels in the BM harvested from the treated (+Dox) versus untreated (–Dox) Id1 shRNA–BMT mice. Data are means ± SD; $n = 10$ per group. (**F**) FACS analysis of the circulating EPCs (c-$kit^+$VEGFR2$^+$$CD11b^-$) in peripheral blood of untreated (–Dox) and treated (+Dox) Id1 shRNA–BMT mice (day 21). A total of $1 \times 10^6$ cells were analyzed per animal. Data are means ± SD; $n = 10$ per group. Note, that because FACS did not detect GFP expression, circulating EPC levels in the peripheral blood were determined in the context of c-Kit expression as described (*21*). (**G**) CD31 staining showing the vascularization defects in pulmonary metastases in treated (+Dox) versus untreated (–Dox) Id1 shRNA–BMT animals (day 28). Scale bar, 100 μm. Dotted line separates the $RFP^+$ metastases from the host lung.

BMT animals [32 ± 7 in –Dox versus 33 ± 6 in +Dox (Fig. 4A)]. This reduction was due primarily to a decrease in macrometastases in Dox-treated Id1 shRNA–BMT animals [13.8 ± 6.1 in –Dox versus 0.6 ± 1.3 in +Dox, $P = 0.0014$ (Fig. 4B)]. No significant reduction in micrometastases was observed in the lungs of these animals (Fig. 4C), which suggested that the inducible Id1 suppression did not affect initial lung colonization by tumor cells, but impaired their progression into macrometastases. Furthermore, tumor-bearing Id1 shRNA–BMT mice treated with Dox outlived the untreated mice [$P = 0.0233$ (Fig. 4D)]. Necropsy revealed that the untreated mice had collapsed lungs containing numerous macrometastatic lesions (Fig. 4D, insert –Dox), which suggested that pulmonary macrometastasis was the main cause of death.

Inducible suppression of Id1 gene expression in vivo was confirmed by quantitative real-time polymerase chain reaction (RT-PCR), which showed a reduction in Id1 mRNA levels in the BM of the Dox-treated Id1 shRNA–BMT mice to one-fifth those of untreated mice (Fig. 4E). More important, conditional Id1 suppression resulted in reduction in the level of circulating EPCs (c-kit$^+$VEGFR2$^+$CD11b$^-$) to one-third the circulating EPCs in those without doxycycline (Fig. 4F). The reduction in EPCs was specific, as we detected no significant change in the levels of BM-derived hematopoietic cells, including B cells, T cells, and myeloid and VEGFR1$^+$ cells (figs. S6 to S8). Our data also suggest that a decrease in lymphocytes in resting Id1 knockout mice recently reported by Nimer and colleagues (*16*) was most likely due to developmental compensations associated with the knockout mice. Overall, our study provides evidence that BM-derived EPCs play a direct role in angiogenesis-mediated progression of metastatic lesions, but they have no effect on metastatic initiation, which is dependent on VEGFR1$^+$ cells. Notably, impaired mobilization of EPCs resulted in a dramatic reduction in vessel density in metastatic lesions in Dox-treated Id1 shRNA–BMT mice [22.2 ± 4.7% in –Dox versus 4.1 ± 2.9% in +Dox (Fig. 4G)]. Although we have observed that a reduction in the levels of circulating EPCs correlates with impaired angiogenesis, our study does not address whether local lung resident progenitors or dedifferentiation of committed hematopoietic cells also contribute to EPC population as reviewed in (*17*).

This study illustrates the critical role of EPCs as novel regulators of the angiogenic switch in metastatic progression and points to a direct role of Id1 in mediating EPC mobilization and recruitment. Although only 12% of the neovessels in the metastatic lesions showed luminal incorporation by BM-derived endothelial cells, it is noteworthy that blocking EPC mobilization caused severe angiogenesis inhibition and significantly impaired the formation of lethal macrometastases, which suggested that EPCs may have additional proangiogenic properties in mediating the angiogenic switch. Notably, gene expression analysis of FACS-purified EPCs from tumor tissue revealed up-regulation of a variety of key proangiogenic genes including growth factors, receptors, chemokines, and ECM modifiers (table S1). Together, these findings support the rationale for the anti-angiogenic treatment of metastatic cancer and suggest that the efficacy of antiangiogenic inhibitors currently used in clinical trials, such as blocking antibodies to VEGF and VEGFR2, may be a consequence of directly targeting BM-derived EPCs, as well as the nascent tumor vasculature. This hypothesis is bolstered by studies that have shown that antiangiogenic drugs also suppress the mobilization and levels of EPCs (*18*). Given that BM-derived endothelial cells also contribute to vessels in humans (*19*, *20*) and that initial metastatic colonization has usually occurred by the time of the primary tumor diagnosis, our results suggest that targeting BM-derived EPCs, perhaps in combination with conventional chemotherapeutics, may provide a feasible therapeutic approach for cancer patients with lung metastases. It is important to note, however, that in the clinical setting it can sometimes take years for dormant micrometastases to progress to lethal micrometastases, a time course that is not recapitulated in our mouse models.

### References and Notes


1. R. N. Kaplan *et al.*, *Nature* **438**, 820 (2005).
2. S. Hiratsuka, A. Watanabe, H. Aburatani, Y. Maru, *Nat. Cell Biol.* **8**, 1369 (2006).
3. J. L. Townson, A. F. Chambers, *Cell Cycle* **5**, 1744 (2006).
4. L. Holmgren, M. S. O'Reilly, J. Folkman, *Nat. Med.* **1**, 149 (1995).
5. G. N. Naumov, L. A. Akslen, J. Folkman, *Cell Cycle* **5**, 1779 (2006).
6. Materials and methods are available as supporting material on *Science* Online.
7. H. G. Kopp, C. A. Ramos, S. Rafii, *Curr. Opin. Hematol.* **13**, 175 (2006).
8. D. J. Nolan *et al.*, *Genes Dev.* **21**, 1546 (2007).
9. L. Laitinen, I. Virtanen, L. Saxen, *J. Histochem. Cytochem.* **35**, 55 (1987).
10. A. G. Arroyo, J. T. Yang, H. Rayburn, R. O. Hynes, *Cell* **85**, 997 (1996).
11. B. Garmy-Susini *et al.*, *J. Clin. Invest.* **115**, 1542 (2005).
12. H. Jin *et al.*, *J. Clin. Invest.* **116**, 652 (2006).
13. D. Lyden *et al.*, *Nat. Med.* **7**, 1194 (2001).
14. M. B. Ruzinova *et al.*, *Cancer Cell* **4**, 277 (2003).
15. K. Hochedlinger, Y. Yamada, C. Beard, R. Jaenisch, *Cell* **121**, 465 (2005).
16. V. Jankovic *et al.*, *Proc. Natl. Acad. Sci. U.S.A.* **104**, 1260 (2007).
17. G. A. Prindull, E. Fibach, *Exp. Hematol.* **35**, 691 (2007).
18. P. Beaudry *et al.*, *Clin. Cancer Res.* **11**, 3514 (2005).
19. B. A. Peters *et al.*, *Nat. Med.* **11**, 261 (2005).
20. S. Jiang *et al.*, *Proc. Natl. Acad. Sci. U.S.A.* **101**, 16891 (2004).
21. F. Bertolini, Y. Shaked, P. Mancuso, R. S. Kerbel, *Nat. Rev. Cancer* **6**, 835 (2006).



22. We thank R. Jaenisch, L. Eisenbach, R. Dickins, S. Elledge, R. Benezra, and D. Trono for reagents and R. Stephen for technical assistance. Supported by funds from the NIH, Robert I. Goldman Foundation, and the Berkowitch Foundation.


### Supporting Online Material

www.sciencemag.org/cgi/content/full/319/5860/195/DC1
Materials and Methods
SOM Text
Figs. S1 to S8
Table S1
References


7 September 2007; accepted 28 November 2007
10.1126/science.1150224


# Dendritic Cell–Induced Memory T Cell Activation in Nonlymphoid Tissues


**Linda M. Wakim,[1] Jason Waithman,[1] Nico van Rooijen,[2] William R. Heath,[3]* Francis R. Carbone[1]***



**Secondary lymphoid organs are dominant sites of T cell activation, although many T cells are subsequently retained within peripheral tissues. Currently, these nonlymphoid compartments are viewed as sites only of effector T cell function, without the involvement of renewed induction of immunity via the interactions with professional antigen-presenting cells. We describe a method of reactivation of herpes simplex virus to examine the stimulation of tissue-resident T cells during secondary challenge. The results revealed that memory CD8$^+$ T cell responses can be initiated within peripheral tissues through a tripartite interaction that includes CD4$^+$ T cells and recruited dendritic cells. These findings lend evidence for the existence of a sophisticated T cell response mechanism in extra-lymphoid tissues that can act to control localized infection.**


The activation of T cells during localized infection takes place within the draining lymph nodes, where the bulk of T cell priming is thought to occur (*1*). However, peripheral nonlymphoid tissues harbor a sizable proportion of the overall T cell pool, primarily consisting of long-lived memory T cells (*2*, *3*). During infection, peripheral tissues invariably represent the first point of contact with a wide range of pathogens, with resident T cells considered as critical to local infection control (*4*). Indeed, it has been suggested that such sites should be viewed as an extension of the secondary lymphoid compartment, and the term effector-lymphoid tissue (ELT) has been used in their description (*5*). Nevertheless, the contribution of the individual components within the ELT


[1]Department of Microbiology and Immunology, University of Melbourne, Melbourne, Victoria 3010, Australia. [2]Faculty of Medicine, Department of Molecular Cell Biology, Vrije Universiteit, 1081 BT, Amsterdam, Netherlands. [3]Division of Immunology, Walter and Eliza Hall Institute of Medical Research, Melbourne, Victoria 3050, Australia.

*To whom correspondence should be addressed. E-mail: fcarbone@unimelb.edu.au (F.R.C.); heath@wehi.edu.au (W.R.H.)